Paediatric phantom dose study using digital radiography with variation of exposure parameters and filtration

Poster No.: C-0986

Congress: ECR 2018

Type: Scientific Exhibit

Authors: L. J. O. Lanca[1], M. W. Bowdler[2], J. Creedon[3], V. Dayer[4], N. Stensholt[5], V. Stuivenberg[6], S. Pinhao[1], M. Visser[6], J. A. Pires Jorge[4]; [1]Lisbon/PT, [2]Salford/UK, [3]Dublin/IE, [4]Lausanne/CH, [5]Oslo/NO, [6]Groningen/NL

Keywords: Radiographers, Radioprotection / Radiation dose, Pediatric, Conventional radiography, Experimental, Digital radiography, Diagnostic procedure, Experimental investigations, Safety, Trauma, Education and training

DOI: 10.1594/ecr2018/C-0986

Aims and objectives

Paediatric digital radiography remains a challenge for many radiographers (Goske, 2011). The subsequent need for focused paediatric care is outlined by 'The Image Gently Campaign' (Strauss, 2015), which reports a lack of both expertise and educational resources surrounding this area. This requirement is reinforced by The International Commission on Radiological Protection (ICRP), which identifies a need for both optimisation and consistence in digital paediatric imaging (Clement, 2013). Although a considerable proportion of recent research surrounds paediatric diagnostic imaging, Jones et. al highlights an absence of literature regarding optimisation in paediatric extremity imaging (Jones, 2015).

This is of particular importance when considering paediatric patients who, due to their additional life expectancy and increased tissue radio-sensitivity, are considerably more sensitive to the detrimental effects of ionising radiation (Berger, 2016). Although the radiation dose received for diagnostic purposes is low, it is pertinent that each exposure be minimised due to the cumulative nature of radiation.

The question to be addressed through our study is as follows; using a paediatric phantom with multiple bone fractures, could the variation of exposure parameters and filtration in Digital Radiography achieve a reduction in dose without substantially affecting image quality?

This study aims to evaluate the variation of exposure parameters and filtration in image quality and dose in a paediatric phantom study using a digital radiography (DR) wireless detector.

Methods and materials

A Kyoto Kagaku 5-year-old (105cm/20kg) paediatric anthropomorphic phantom (PBU-70B) (Fig. 1 on page 6), was imaged. Fractures were present on the left side of the phantom. Two regions were selected for this study, namely wrist and rib. Wrist fractures are one of the most commonly occurring fractures in paediatric patients and rib fractures have a considerable risk of misdiagnosis (Slovis, 2015).

Imaging System and Positioning

All images were acquired using an Arcoma X-ray imaging system with DAP integration. The X-ray tube has the option to add 0.1, 0.2 or 0.3mm Cu filtration. All images were acquired on the same indirect Canon DR detector (CXDI-701C Wireless General Purpose) with a caesium iodide scintillator with a detective quantum efficiency (DQE) of >70%. This detector has a pixel size of 125x125µm and an image matrix size of 2800x3408 pixels, with an effective imaging area of 35x43cm. The resolution of the detector is 4.0lp/mm with 4096 gradations. No anti-scatter grid was used during this study, as this would increase patient dose (Fritz, 2014).

The phantom was imaged in the supine position for both antero-posterior (AP) and oblique rib projections. For the oblique projection, a radiolucent pad was placed beneath the phantom, positioning the phantom at 20-degrees obliquity. The collimated field remained constant at 15x26cm, with a source-to-image-distance (SID) of 110cm. Dorso-palmar (DP) and lateral standard wrist projections were also acquired, with the collimated field fixed at 14.5x8cm and an SID of 110cm (Knight, 2014). A small focal spot was used for both wrist projections, while a large focal spot was used for both rib projections.

Protocol

A total of 36 images were acquired, nine for each projection. Three separate image acquisition dose protocols were used; low, medium and high. The high dose protocol employed standard exposure parameters, with tube potentials of 48kV and 52kV for the DP and lateral wrist projections, respectively. A tube intensity time product of 2mAs was applied for both DP and lateral wrist projections, when this was used (Knight, 2014). The high dose protocol employed 60kV and 0.63mAs for the AP rib projection and 68kV and 3.2mAs for the oblique rib projection (Berger, 2016). For each projection, the mAs was then lowered in two separate steps and low and medium protocols were constructed (Table 1 on page 7). For each protocol, the effect of Cu filtration was assessed using no filtration as well as 0.1mm and 0.2mm added Cu filtration.

Dose measurement

Dose Area Product (DAP) values were derived using a calibrated integrated ionization chamber. DAP was then used to calculate the Entrance Skin Dose (ESD) for each exposure, using equation 1.

$$ESD = (DAP/A)*BSF \quad (Eq.1)$$

The area of the collimated field is represented by A and the backscatter factor is represented by BSF. The backscatter factor used throughout this study was 1.3 (Toivonen, 2001)

Image quality

Physical measurement

Contrast-to-noise ratio (CNR) was used to determine a physical measurement of image quality. CNR assesses the effect of changes in beam quality on image quality. ImageJ (Burger, 2008) was used to define regions of interest (ROIs) for CNR calculations. Four ROIs were placed on homogenous regions within each of the 36 total images, two on soft tissue and two on bone (Fig. 2 on page 8). For the two ROIs placed on soft tissue and the two placed on bone, a mean value was calculated to get more reliable measurements. CNR was then calculated using equation 2:

$$CNR=(S1-S2)/\#_1 \quad \text{(Eq.2)}$$

where, S1 represents the mean pixel value within the ROIs placed on bone, and S2 represents the mean pixel value within the ROIs placed on soft tissue. The $\#_1$ represents the standard deviation of bone (Jones, 2015; Mori, 2013).

Observers

Fifteen observers assessed visual image quality for each image through visual grading analysis (VGA). The observer group consisted of thirteen Radiography students of varying levels (years 1-4), as well as two experienced radiographers. ViewDEX was used to display the images, illustrate visual scoring criteria and also collect observer scores (Svensson, 2010). Prior to image-viewing, the observers were trained in the visual assessment task in order to maximise validity and reliability. The observers could pan and zoom, but the use of windowing was prohibited. They were made aware of the fracture location prior to rating the images. The observers first scored the eighteen wrist images, followed by a short break, before scoring the eighteen rib images. All images were randomized and observers were blinded to acquisition conditions and exposure factor information. A five-point Likert scale was used to assess five criteria: overall image quality, contrast, sharpness, noise and fracture visibility. With this scale, a score of 1 indicates Poor, while that of 5 indicates Excellent. Numerical scales as such are often used to simplify information and to improve inter-observer agreement (Svensson, 2010). Ambient lighting conditions in the observation room remained constant throughout the image-viewing process at less than 10 lux (Park, 2008; Brennan, 2007). The monitor used for observer analysis was also fixed throughout the study, with an area of 32.4x43.2cm.

Images were displayed on a 21.3-inch Monochrome LCD monitor MS25i2 (ML21025), manufactured by TotokuTM, calibrated to the DICOM greyscale standard (McGinty,

2013). All observer information was anonymised. The total VGA (VGA_T) was calculated using equation 3:

$VGA_T=(\#_{O,I}S_C)/N_iN_o$ (Eq. 3)

where, S_C represents each criterion score given by the observers, O represents the observer and I represents the image. N_i represents the total number of images and N_o is the total number of observers (Mansson, 2000). A separate VGA score was calculated using the three primary visual image quality parameters; contrast, sharpness and noise (VGA_{CSN}). This score was calculated by adding the observer scores from these three criteria and generating a mean value. The VGA_{CSN} was then correlated with fracture visibility for each projection.

Statistics

Descriptive statistics were used to analyse the data. This data was imported to Statistical Package for the Social Sciences (SPSS). Mean VGA, CNR and R2 correlations were calculated using Excel. A very high correlation is noted between 0.90 and 1, while a high correlation is between 0.70 and 0.90. A moderate correlation is seen between 0.50 and 0.70 (Mukaka, 2012). An independent samples Kruskal-Wallis non-parametric test was used to analyse statistically significant differences at 95% confidence level between the 15 observers regarding VGA.

Images for this section:

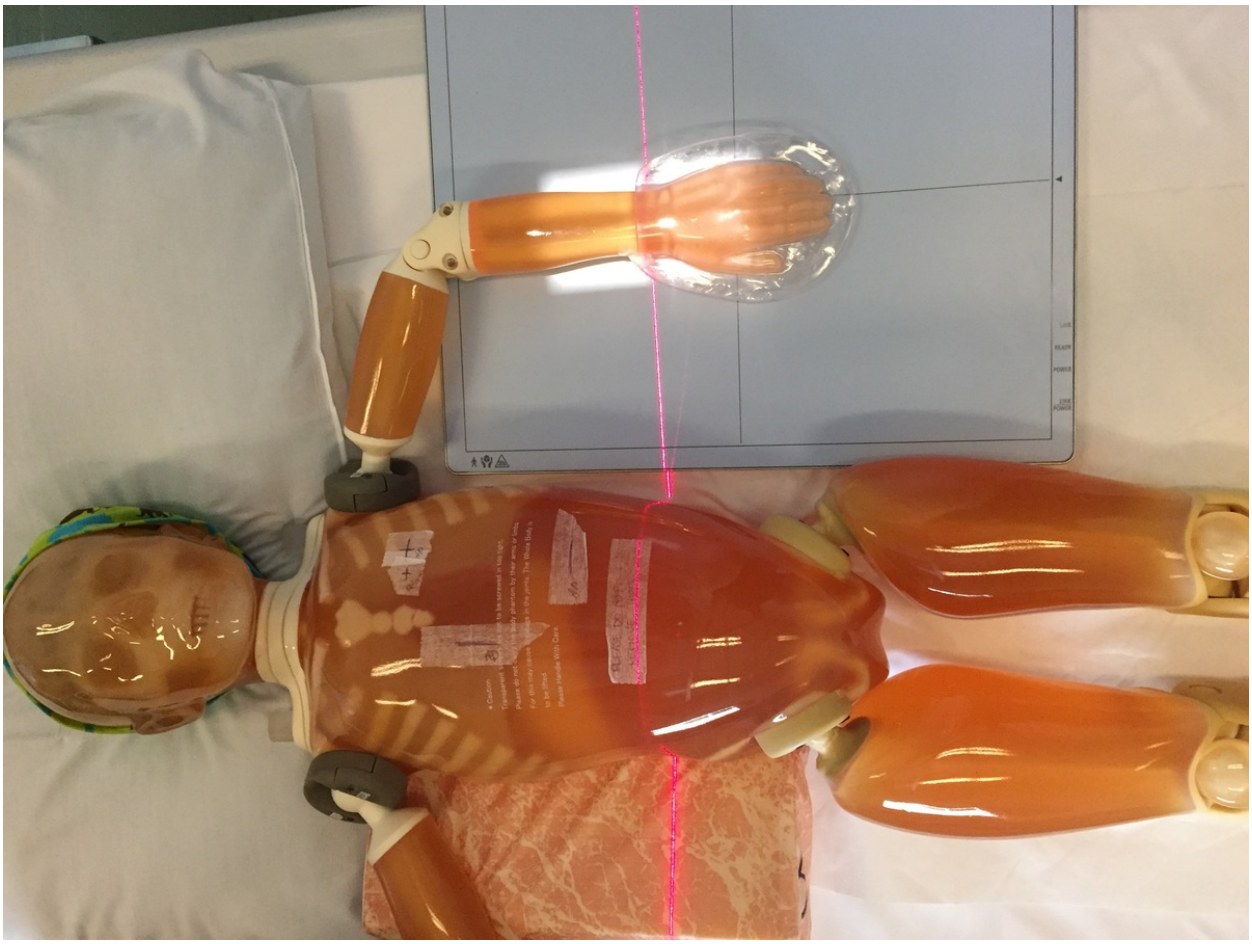

Fig. 1: Experimental setup for wrist dorso-palmar view using Kyoto Kagaku 5-year-old (105cm/20kg) paediatric anthropomorphic phantom (PBU-70B)

Dose level	anatomic views	Incidences	kV	mAs	Cu Filter
low	Wrist	Dorso-palmar	48	0,5	none
					0,1mm
					0,2mm
		Lateral	52	0,5	none
					0,1mm
					0,2mm
	Ribs	AP	60	0,4	none
					0,1mm
					0,2mm
		Oblique	68	2	none
					0,1mm
					0,2mm
medium	Wrist	Dorso-palmar	48	1	none
					0,1mm
					0,2mm
		Lateral	52	1	none
					0,1mm
					0,2mm
	Ribs	AP	60	0,5	none
					0,1mm
					0,2mm
		Oblique	68	2,5	none
					0,1mm
					0,2mm
High (Standard protocol)	Wrist	Dorso-palmar	48	2	none
					0,1mm
					0,2mm
		Lateral	52	2	none
					0,1mm
					0,2mm
	Ribs	AP	60	0,63	none
					0,1mm
					0,2mm
		Oblique	68	3,2	none
					0,1mm
					0,2mm

Table 1: Image acquisition protocols

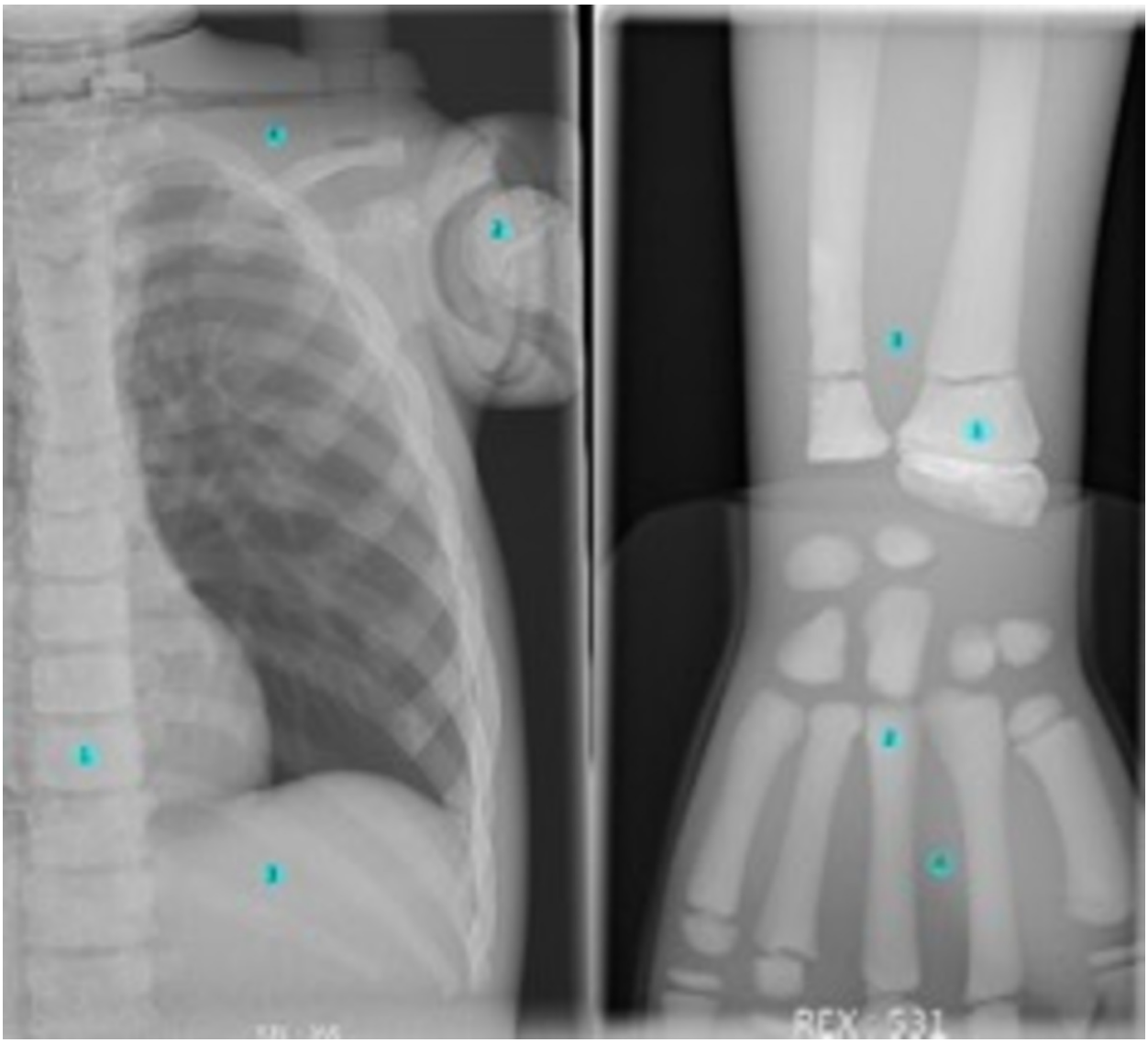

Fig. 2: ROIs for the rib AP (left) and wrist DP (right) views with ROI 1 and 2 on bone and ROI 3 and 4 on soft tissue

Results

The protocols for wrist with dose and image quality measures are presented in Table 2 on page 11: CNR, DAP, ESD and VGA_T. As expected, dose measurements and CNR decreased with added filtration. The average reduction for all three filters was identical for DP and lateral wrist projections, at 76%. The most substantial reduction in image quality occurred with 0.2mm added Cu filtration. Overall, the addition of filtration reduced dose for all projections, however this results in an overall reduction in image quality. VGA_T is lower with the addition of filtration.

Table 3 on page 12 demonstrates the results for ribs with regards to CNR, DAP, ESD and VGA_T. The primary focus of this table is on AP and oblique rib projections and again, both dose and CNR values decreased with added filtration. For the AP rib projection, with no added filtration, there was a 36% dose decrease from high to low dose protocols, with an equal decrease between both high and medium, and medium and low dose protocols. However, the VGAT differed by merely 0.1 between high and low dose protocols with no added filtration. When 0.1mm Cu filtration was added, there was a comparable dose decrease of 36% between high and low dose protocols, with an 18% decrease between high and medium dose protocols, and a 22% decrease between medium and low dose protocols. However, the VGA_T differed by just 0.3 between high and low dose protocols with 0.1mm added filtration. With 0.2mm added Cu filtration, there was a similar dose decrease of 38% from high to low dose protocols, with a 19% decrease between high and medium protocols and a 23% decrease between medium and low dose protocols. Again, the VGA_T differed by just 0.3 between high and low dose protocols, with 0.2mm added filtration.

For the oblique rib projection, with no added filtration, there was a 37% dose decrease from high to low dose protocols, with a reduction of just 0.2 in VGA_T. When 0.1mm Cu filtration was added, there was a similar 37% reduction in dose, with an increase of 0.1 in VGAT. With 0.2mm added filtration, there was a dose decrease of 38% and a reduction of just 0.3 in VGA_T. A dose variation of 20-22% was found between high and medium, and medium and low dose protocols, for all three filtration settings for all three dose protocols.

Dose measurements

Fig. 3 on page 13 demonstrates the combined mean ESD for the high, medium and low dose protocols for wrist and ribs. As expected, the highest doses were recorded using the high dose protocol. The dose levels ranged from 8.09-28.23µGy, from 10.85-38.27µGy and from 15.31-55.15µGy for the low, medium and high dose protocols, respectively.

There was an overall decrease in ESD with added Cu filtration, as seen in Figure 3. There was a 51.8% reduction in ESD when 0.1mm Cu filtration was added, with the low dose protocol. The entrance surface dose was reduced by 47.7% and by 53.0% for the medium and high dose protocols, respectively. A greater dose reduction was achieved with 0.2mm added Cu filtration, at 71.4%, 71.6% and 72.2% for the low, medium and high dose protocols.

Contrast-to-Noise Ratio measurements

The mean CNR for each projection and for each of the three dose protocols is displayed in Fig. 4 on page 13. A wide range is seen in CNR values for both wrist projections, with that of the DP wrist varying between 3.7 and 16.2 and that of the lateral wrist varying between 6.9 and 16.3. The difference between CNR values for both rib projections, however, is much less varied, ranging between 2.9 and 5.9 for the AP projection, and 1.5 and 2.3 for the oblique projection. As expected, the CNR for all exposures decreased with increased filtration, for all three dose protocols.

Visual and Physical Image Quality Measurements

For each of the four projections, the fracture visibility scores were correlated with both physical (CNR) and visual measurements (VGA_{CSN}) (Table 4 on page 14). A strong correlation was found between CNR and fracture visibility for both DP and lateral wrist projections. CNR and fracture visibility for the AP rib projection also shows a strong correlation. Regarding the oblique rib projection, a moderate correlation was found between CNR and fracture visibility. Similar findings can be seen in the relationship between VGA_{CSN} and fracture visibility, with the strongest correlations occurring in the DP wrist, lateral wrist and AP rib projections. The weakest correlation was found in the oblique rib projection.

The distribution of mean ratings was the same across all fifteen observers, showing no significant statistical difference in VGA_T score between observers ($p=0.450$). A strong correlation was found between the physical measurement of CNR and the visual analysis of each image. This correlation was weaker for the oblique rib view than for the remaining three projections.

Images for this section:

Wrist	Projections	kV	mAs	Cu Filter	CNR	DAP (mGy/cm²)	ESD (µGy)	VGA_T
Low	Dorso-palmar	48	0,5	none	10,4	0,7	7,84	3,5
				0,1mm	5,5	0,3	3,36	2,5
				0,2mm	3,7	0,1	1,12	1,7
	Lateral	52		none	13,3	0,9	10,09	3,1
				0,1mm	10	0,3	3,36	2,4
				0,2mm	6,9	0,2	2,24	1,8
Medium	Dorso-palmar	48	1	none	14,4	1,4	15,69	3,8
				0,1mm	8,3	0,5	5,6	3,1
				0,2mm	5,5	0,3	3,36	2,3
	Lateral	52		none	15,1	1,7	19,05	3,8
				0,1mm	12	0,8	8,97	3,1
				0,2mm	10	0,3	3,36	2,4
High	Dorso-palmar	48	2	none	16,2	2,8	31,38	4,2
				0,1mm	11,4	1,1	12,33	3,3
				0,2mm	7,6	0,5	5,6	3,1
	Lateral	52		none	16,3	3,5	39,22	4,1
				0,1mm	15,6	1,4	15,69	3,7
				0,2mm	11,4	0,8	8,97	3,1

Table 2: Wrist protocol with dose and image quality measurements

Ribs	Projections	kV	mAs	Cu Filter	CNR	DAP (mGy/cm²)	ESD (µGy)	VGA_T
Low	AP	60	0,4	none	4,7	3,9	13	3
				0,1mm	3,9	1,8	6	2,6
				0,2mm	2,9	1	3,33	2,2
	Oblique	68	2	none	2,3	24,6	82	3,5
				0,1mm	1,8	12,5	41,67	3,4
				0,2mm	1,5	7,7	25,67	3,1
Medium	AP	60	0,5	none	5	4,9	16,33	3,1
				0,1mm	4,1	2,3	7,67	2,9
				0,2mm	3,5	1,3	4,33	2,5
	Oblique	68	2,5	none	2,2	30,6	102	3,7
				0,1mm	1,9	15,6	52	3,4
				0,2mm	1,5	9,7	32,33	3,1
High	AP	60	0,63	none	5,9	6,1	20,33	3,5
				0,1mm	4,6	2,8	9,33	2,8
				0,2mm	3,6	1,6	5,33	2,7
	Oblique	68	3,2	none	2,3	38,9	129,67	3,7
				0,1mm	1,8	19,9	66,33	3,3
				0,2mm	1,6	12,4	41,33	3,4

Table 3: Ribs protocol with dose and image quality measurements

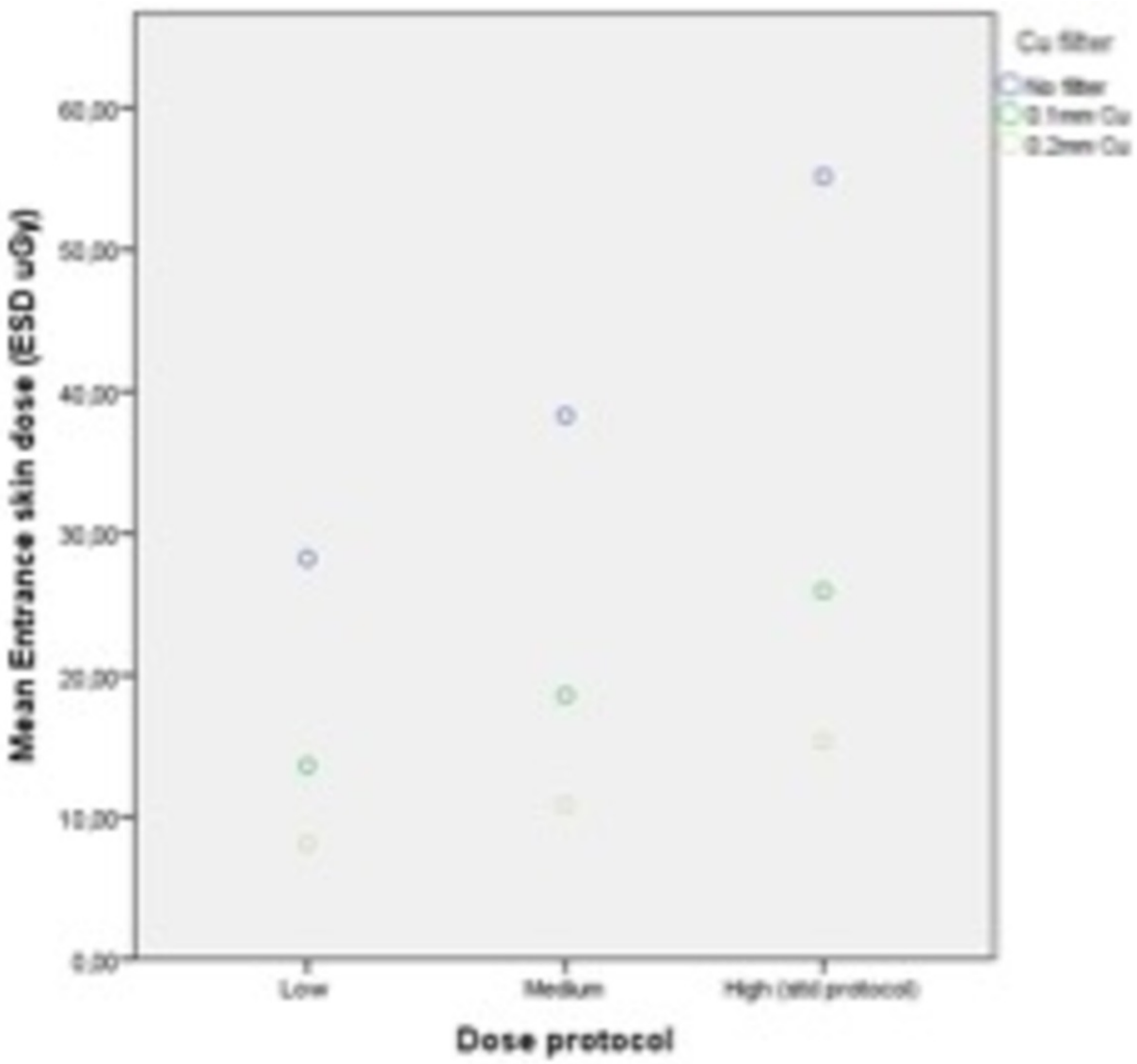

Fig. 3: Mean ESD for each protocol and Cu filtration

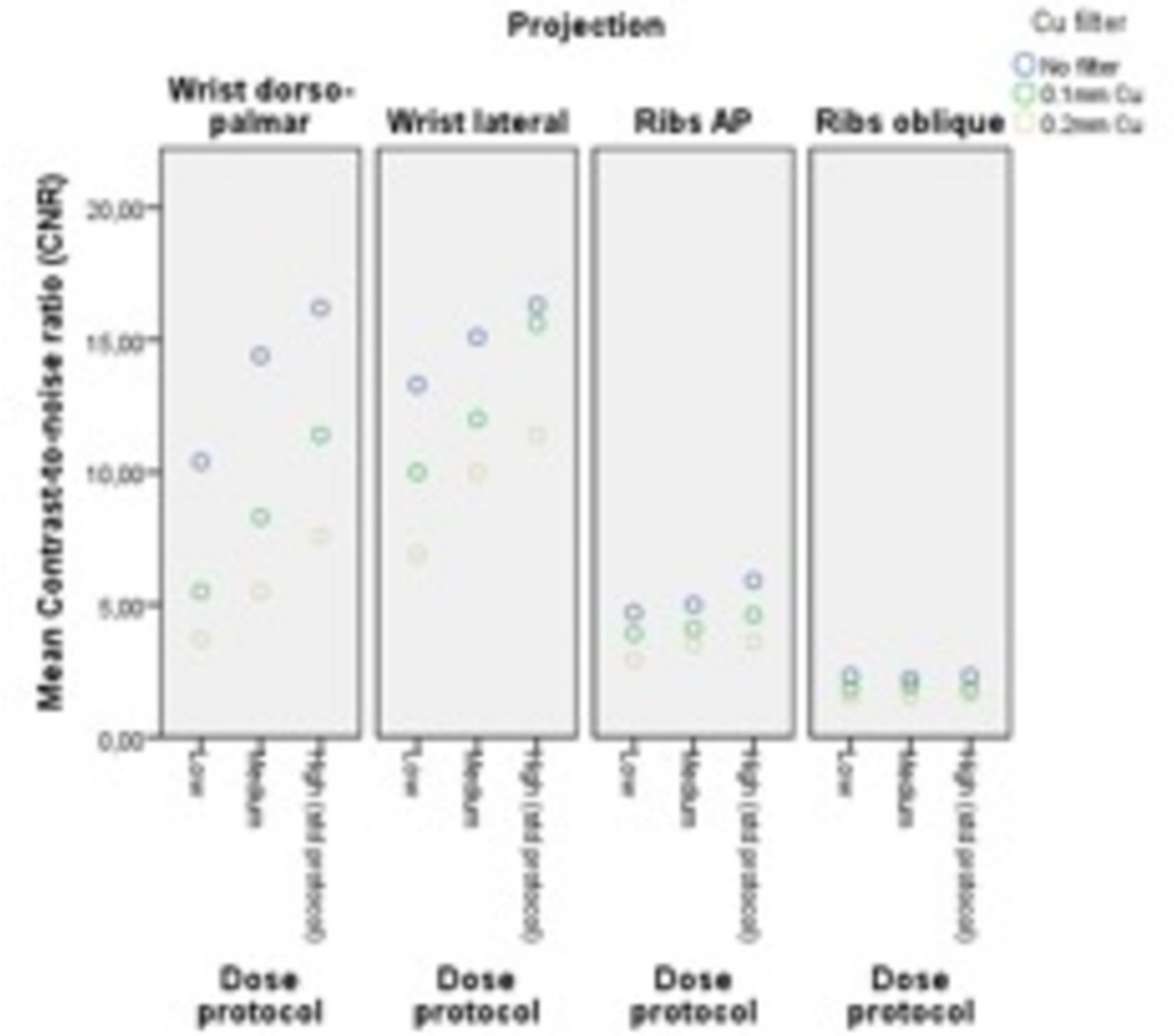

Fig. 4: Mean CNR for each protocol and Cu filtration level

Projection	CNR vs Fracture Visibility	VGA_{CSN} vs Fracture Visibility
DP Wrist	0.7697	0.8908
Lateral Wrist	0.9067	0.9477
AP Ribs	0.7917	0.8577
Oblique Ribs	0.5384	0.6970

Table 4: R2 correlation coefficients between CNR, VGACSN and fracture visibility

Conclusion

The results of this study show a strong correlation between visual and physical measurements for each projection, reinforcing our findings. This strong correlation poses the question: Are both physical and visual measurements needed for image quality analysis? Similarly, overall image quality scores were similar to VGA_{CSN} values, suggesting that overall image quality may be sufficient for predicting fracture visibility and image quality. Similar outcomes were found in other studies (Lança, 2013). The standard deviation for inter observer assessment is low, meaning that observers agreed with one another about each criterion.

The most striking result found in this study was the effect of Cu filtration on both dose and image quality, with added filtration consistently reducing patient dose, at the cost of image quality. The values for ESD and DAP found in this study mirror those found in published research (Slovis, 2015; Knight, 2014).

The primary focus of this study was on wrist and rib fractures as wrist fractures are among the most common paediatric fractures (Rennie, 2007), and rib fractures are associated with high rates of misdiagnosis (Slovis, 2015). In cases of abuse, however, many fractures occur in the ribs, the most acute of which are frequently missed on initial imaging. This constitutes an important topic for further research in the clinical context, regarding the optimization of exposure in the paediatric population.

The results of this research are valid in the context of this study and this constitutes the major limitation as cannot be valid in the clinical context. Although it has been well documented that DR detectors allow the production of good quality images at low exposures due to their high associated DQE, further research is suggested in clinical practice, using real paediatric patients.

Furthermore, different hospitals may use different positioning methods, detectors and parameters for paediatric patients, when compared to those used throughout this study. However, this does not mean that the parameters used in this study cannot be adapted and applied in clinical practice.

Using digital radiography, the variation of exposure parameters can achieve a reduction in dose, without impairing diagnostic image quality or fracture visibility. Superior image quality can be achieved for DP and lateral wrist projections at higher doses, without the use of Cu filtration. However, the addition of Cu filtration for the rib projections can reduce phantom dose with almost no impact on overall image quality. Overall, the addition of filtration reduced dose for all projections.

Personal information

Luís Lança has been teaching radiography subjects since 2000 at Lisbon School of Health Technology (ESTeSL/Portugal). His teaching and research activities involve expertise, knowledge and practical skills in contemporary diagnostic radiography practice (such as plain digital radiography, Computed Tomography and radiation protection). Luís is also an Affiliated Senior Research Specialist in Radiography at Karolinska Institutet/ Sweden.

This work was undertaken during the radiography research summer school OPTIMAX 2017, held in the Oslo and Akershus University College of Applied Sciences, Oslo/ Norway 2017 All the co-authors are participants in the 5th OPTIMAX edition representing several higher eduction institutions across Europe.

References

Berger RP, Panigrahy A, Gottschalk S, Sheetz M. Effective Radiation Dose in a Skeletal Survey Performed for Suspected Child Abuse. J Pediatr. Elsevier Inc.; 2016;171:310-2.

Brennan PC, McEntee M, Evanoff M, Phillips P, O'Connor WT, Manning DJ. Ambient lighting: effect of illumination on soft-copy viewing of radiographs of the wrist. AJR Am J Roentgenol. 2007;188(2):177-80.

Burger W, Burge M. Digital Image Processing: An Algorithmic Introduction Using Javae. 2008. p. 2.

Clement C, Sasaki M, Khong P-L, Ringertz V, Donoghue D, Frush M, et al. ICRP, 2013. Radiological Protection in Paediatric Diagnostic and Interventional Radiology. Compend Dose Coefficients based ICRP Publ 60. 2012;42(2):130.

Fritz S, Jones AK. Guidelines for anti-scatter grid use in pediatric digital radiography. Pediatr Radiol. 2014;44(3):313-21.

Goske MJ, Charkot E, Herrmann T, John SD, Mills TT, Morrison G, et al. Image Gently: challenges for radiologic technologists when performing digital radiography in children. Pediatr Radiol. 2011;41(5):611-9.

Jones A, Ansell C, Jerrom C, Honey ID. Optimization of image quality and patient dose in radiographs of paediatric extremities using direct digital radiography. Br J Radiol. 2015;88(1050):20140660.

Knight SP. A paediatric X-ray exposure chart. J Med Radiat Sci. 2014;61(3):191-201.

Lanca, Luis; Silva A. Digital Imaging Systems for Plain Radiography. New York: Springer; 2013. 173 p.

Mansson LG. Methods for the Evaluation of Image Quality: A Review. Radiat Prot Dosimetry. 2000;90(1):89-99.

McGinty, G, Allen B, Wald C. Imaging 3.0 ACR IT Reference Guide for the Practicing Radiologist. Am Coll Radiol. 2013;1-11.

Mori M, Imai K, Ikeda M, Iida Y, Ito F, Yoneda K, et al. Method of measuring contrast-to-noise ratio (CNR) in nonuniform image area in digital radiography. Electron Commun Japan. 2013;96(7):32-41.

Mukaka MM. A guide to appropriate use of Correlation coefficient in medical research. Malawi Med J. 2012;24(3):69-71.

Park CM, Lee HJ, Goo JM, Han DH, Kim JH, Lim KY, et al. Comparison of observer performance on soft-copy reading of digital chest radiographs: High resolution liquid-crystal display monitors versus cathode-ray tube monitors. Eur J Radiol. 2008;66(1):13-8.

Rennie L, Court-Brown CM, Mok JYQ, Beattie TF. The epidemiology of fractures in children. Injury. 2007;38(8):913-22.

Slovis TL, Strouse PJ, Strauss KJ. Radiation Exposure in Imaging of Suspected Child Abuse: Benefits versus Risks. J Pediatr. Elsevier Inc; 2015;167(5):963-8.

Strauss KJ, Frush DP, Goske MJ. Invited Paper Image Gently Campaign#: Making a

World of Difference. Med Phys Int J. 2015;3(2):94-108.

Svensson S, Zachrisson S, Svalkvist A, Ba M, Ha M, Radiology D, et al. View Dex#: an Efficient and Easy-To-Use Softw Are. Radiat Prot Dosimetry. 2010;139(1):42-51.

Toivonen M. Patient dosimetry protocols in digital and interventional radiology. Radiat Prot Dosim. 2001;94(1-2):105-8.